Evolution of a rare sequence of surface transitions with temperature and film thickness

B. K. McCoy,[1,2] LiDong Pan,[1] Z. Q. Liu,[1,3] S. T. Wang,[4] Shun Wang,[1] J. W. Goodby,[5] and C. C. Huang[1]

[1]*School of Physics and Astronomy, University of Minnesota, Minneapolis, Minnesota 55455, USA*

[2]*Department of Mathematics and Physics, Azusa Pacific University, Azusa, California 91702, USA*

[3]*Department of Physics, Astronomy and Engineering Science, St. Cloud State University, St. Cloud, Minnesota 56301, USA*

[4]*Department of Physics, Cornell University, Ithaca, New York 14853, USA*

[5]*Deptartment of Chemistry, University of York, York YO10 5DD, United Kingdom*

In free-standing smectic films, layers near the surfaces of the film often contain molecules tilted away from the layer normal, while in the bulk of the film the magnitude of the tilt decays exponentially with distance from the surface. We have identified the detailed molecular tilt orientations in the surface layers of films for one antiferroelectric liquid crystal compound. A series of five surface structures exists with different nonplanar tilt arrangements for each structure. The molecular orientations in the surface layers evolve with temperature. The polarization of the film also evolves with temperature, corresponding to the tilt arrangements. Using ellipsometric data, we reconstruct the changes in the magnitude and azimuthal direction of the tilt as functions of temperature. We have also studied films of several different thicknesses. We present a phase diagram for the five surface structures showing the dependence on temperature and film thickness.

I. INTRODUCTION

Smectic liquid crystals consist of elongated rigid molecules arranged in molecular monolayers [1]. Positional correlations of the molecules within each layer are liquidlike. Molecular orientations are ordered in smectic phases, with a preferred direction for the molecular long axis in each layer. The director $\hat{n}_j$ specifies the molecular long axis in the jth layer. The projection of $\hat{n}_j$ on the layer plane is defined as the vector $\vec{c}_j$. $\hat{n}$ and $\vec{c}$ may vary from layer to layer, giving rise to a variety of smectic phases. In the smectic-*A* (Sm*A*) phase, $\hat{n}$ is parallel to the layer normal for all layers. When the molecules are tilted so that $\hat{n}$ is not parallel to the layer normal, the phase is denoted as smectic-*C* (Sm*C*). The azimuthal orientation of $\hat{n}$ may also vary from layer to layer in Sm*C* variant phases.

In free-standing smectic films, suppression of thermal fluctuations by surface tension [2] may cause the tilts in surface layers to be more ordered than in the bulk. For example, the bulk of a film may be in the Sm*A* phase while the surface layers contain Sm*C*-like tilted molecules. Such tilted surface layers are easily observed by optical techniques because the Sm*A* bulk is optically uniaxial while the surface layers are biaxial. Previous studies of Sm*A* films with tilted surface layers have shown that the surface tilt arrangements may be planar [3–6] or nonplanar [7,8]. Planar arrangements may be synclinic, in which $\vec{c}$ is parallel for surface layers on opposite sides of the film, or anticlinic, in which opposite $\vec{c}$ vectors are antiparallel. Transitions between synclinic and anticlinic structures can occur with changes in temperature [4,10,11] or application of an electric field [4,6,12]. Nonplanar structures have been observed with the $\vec{c}$ vectors for outermost layers being nonplanar [7] or with the $\vec{c}$ vectors for adjacent layers within each surface being nonplanar [8].

In a previous paper [8], we identified the surface tilt orientations while the bulk was in the Sm*A* phase for one antiferroelectric liquid crystal compound, 12OF1M7. Figure 1

shows the chemical structure of this compound. The bulk phase sequence for 12OF1M7 is SmC_A^* (78.4 °C) SmC_{FI1}^* (81.1 °C) SmC_{FI2}^* (84.0 °C) SmC^* (91.3 °C) SmC_α^* (92.4 °C) Sm*A* (106 °C) Isotropic. A 16-layer film of 12OF1M7 was shown to undergo a series of transitions between five distinct surface structures while the bulk of the film was Sm*A*. In this paper, we study the effects on the surface structures with changes in temperature and film thickness for films thick enough to contain a Sm*A* bulk. Very thin films of 2–6 layers, for which all layers of the film are affected by surface effects, were analyzed in Ref. [9]. We do not include films of 7–11 layers because difficulties arising from the transition between surface-dominated behavior and weakly coupled surfaces make the data difficult to interpret. The tilt and azimuthal angles of the molecules within the surface layers vary with temperature. These changes in the tilt structure also produce corresponding changes in the film polarization. We present two mechanisms by which smooth changes in the molecular directions with temperature can cause the polarization to change direction by 180°. The same five surface structures are observed for all films thick enough to contain a Sm*A* bulk region, though some surface structures are missing in thicker films. We present a phase diagram for the five surface structures.

II. EXPERIMENTAL METHODS

The optical biaxiality of surface layers makes them suitable for study by optical techniques. We use null transmission ellipsometry (NTE) [13], in which elliptically polarized
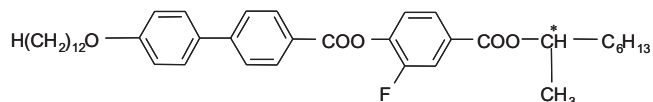
FIG. 1. Chemical structure of 12OF1M7.
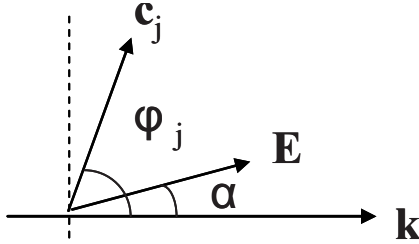
FIG. 2. Definition of angles in the film plane used in the text. **k** is the projection of the wave vector of the incident light on the film plane. **E** is the direction of the applied electric field. $\vec{c}_j$ is the $\vec{c}$ vector of the jth layer.

FIG. 3. These diagrams represent the five surface structures observed in the bulk Sm*A* temperature window. The arrows are the $\vec{c}$ vectors for each layer. Vector lengths and angles are not to scale. The highest temperature surface tilt structure is on the right.

light is transmitted through a free-standing liquid crystal film at an angle of 45° to the film normal. The optical activity of the sample changes the polarization state of the transmitted light. We choose the ellipticity of the incident light such that the transmitted light is linearly polarized. Under any given conditions, two ellipsometric parameters, Ψ and Δ characterize the effect of the sample on the transmitted light. Ψ is the direction of polarization of the linearly polarized transmitted light. Δ is the phase difference between the two perpendicular components of the incident light; Δ is related to the ellipticity of the polarization of incident light.

When chiral molecules, such as molecules of 12OF1M7, are present in a tilted smectic phase, a spontaneous polarization develops [1]. For any smectic layer, the ferroelectric polarization of the layer is perpendicular to $\vec{c}$ and approximately proportional to the magnitude of $\vec{c}$. The film then has a net polarization approximately proportional to the sum of the $\vec{c}$ vectors for each layer. In the following, we do not consider flexoelectric polarization because for the structures studied, the magnitude of the ferroelectric polarization is two or more orders of magnitude larger than the magnitude of the flexoelectric polarization [8]. When an external electric field is present, the net polarization of a film aligns parallel to the field. We apply voltages to eight electrodes arranged in a circle around the sample, producing an electric field in the plane of the film. The strength of the electric field is about 7 V/cm, enough to align the sample's polarization with the field, but too small to distort the film's tilt structure. By varying the voltages on the electrodes, we can choose the direction of the electric field to be at any angle within the film plane. The angle between the electric field and the projection of the incident wave vector on the film plane is defined as α, as shown in Fig. 2. We obtain data of Ψ and Δ as functions of temperature, or as functions of α with temperature held constant.

To analyze our data, we model the sample's optical activity using the 4×4 matrix method [14]. Each layer is assumed to be uniaxial with indices of refraction n_o $= 1.496 \pm 0.003$ perpendicular to the director $\hat{n}$ and n_e $= 1.658 \pm 0.003$ parallel to $\hat{n}$. The layer thickness is d $= 3.66 \pm 0.05$ nm. The values of n_o, n_e, and d were obtained by the technique described in Ref. [15]. For a single layer, Maxwell's equations are applied to an incident electric field to calculate the transmitted electric field. This process is iterated for each layer to calculate the electric field transmitted through the entire film. The ellipsometric parameters Ψ and
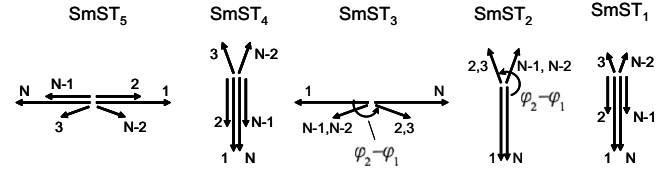
Δ are calculated from the transmitted electric field. The simulations require specification of the tilt (θ) and azimuthal (φ) angles for the molecular orientations in each layer. We search for models of the tilt structures so that the simulations match the data for Ψ and Δ.

III. EVOLUTION OF SURFACE STRUCTURES WITH TEMPERATURE

The surface structures observed in a 16-layer film are summarized in Fig. 3. For convenience, we will refer to these five structures as smectic surface tilt structures (SmST_1-SmST_5). All of these were observed at temperatures above the bulk Sm*A*-SmC_α^* transition. A series of surface transitions occurred from SmST_1 at high temperature to SmST_5 just above SmC_α^*. Each of the five surface structures can be characterized as either synclinic or anticlinic and either ferroelectric or nearly antiferroelectric. We use the terms synclinic and anticlinic to refer to the outermost layers; synclinic (anticlinic) means that $\vec{c_1}$ is parallel (antiparallel) to $\vec{c_N}$ for a film of N layers. There are about three tilted layers at each film surface [16]. We use the terms ferroelectric and antiferroelectric to describe the polarizations of the outermost layer and the neighboring layer. In this paper, ferroelectric (antiferroelectric) means $\vec{c_1}$ is parallel (antiparallel) to $\vec{c_2}$.

SmST_1 is a synclinic ferroelectric structure. SmST_2 remains synclinic, but the second layer switches from ferroelectric to nearly antiferroelectric. At the SmST_2-SmST_3 transition, the outermost layers switch from synclinic to anticlinic. The structure for SmST_4 is synclinic and ferroelectric, just as for SmST_1. The SmST_4-SmST_5 transition is a change from synclinic to anticlinic outermost layers, similar to the SmST_2-SmST_3 transition. All of the structures contain nonplanar tilts in the second or third layers. We have studied films of other thicknesses to examine the dependence of the surface structures on film thickness and temperature. All films with thickness greater than 10 layers exhibited the same five surface tilt structures. The sequence of the surface tilt structures with changes in temperature was the same for all thicknesses, except for some structures missing in some thicknesses.

We have extensively studied SmST_2 and SmST_3 because changes in the tilt and azimuthal angles of these surface structures produce significant changes in the NTE data. Using the 4×4 matrix method, we have obtained the dependence of the surface tilt and the nonplanar angle $\varphi_2 - \varphi_1$ as functions of temperature in SmST_2 and SmST_3. The tilt pro-
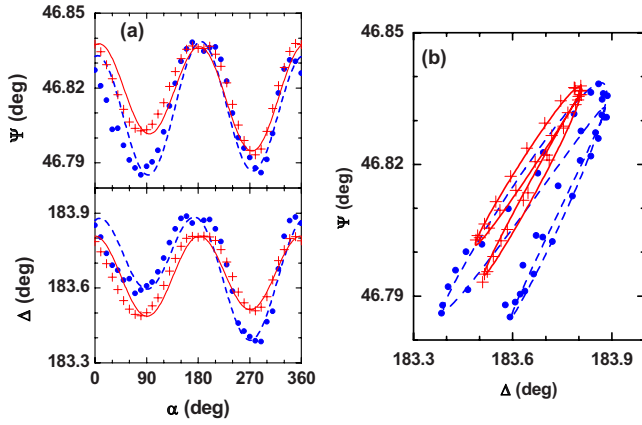
FIG. 4. (Color online) (a) Ψ and Δ vs α for SmST_2 in a 13 layer film. (b) shows Ψ vs Δ. Crosses (circles) represent data and solid (dashed) lines represent simulation results at 94.77 °C (92.54 °C).

file from mean field theory [17] is used for simulations of SmST_2 and SmST_3.

$$\theta_j = \theta_{surf} \frac{\cosh\left(\left[2\left(j - \frac{1}{2}\right) - N\right]/2\xi\right)}{\cosh([N-1]/2\xi)}. \tag{1}$$

Here θ_{surf} is the tilt angle of the outermost layers, ξ is the tilt correlation length, N is the total number of layers in the film, and j represents the jth layer. The outermost layers were synclinic for SmST_2 or anticlinic for SmST_3. The azimuthal angles of the interior layers were taken to be $\varphi_i = \varphi_2$ for $i = 3 \ldots N/2$ and $\varphi_j = \varphi_{N-1}$ for $j = N/2 \ldots N-1$. Each simulation for SmST_2 or SmST_3 had three parameters: θ_{surf}, ξ, and $\varphi_2 - \varphi_1$. Representative data of SmST_2 and SmST_3 are shown in Figs. 4 and 5. SmST_2 has minima in the Ψ vs α and Δ vs α curves at $\alpha = 90°$ and $\alpha = 270°$, while SmST_3 has minima at $\alpha = 0°$ and $\alpha = 180°$. This shows that the outermost layers rotate by 90° at the SmST_2-SmST_3 transition as the structure changes from synclinic to anticlinic. The amplitude of the Ψ vs α and Δ vs α curves determines θ_{surf}. Because Ψ and Δ as functions of α both have two minima, the Ψ vs Δ curves in
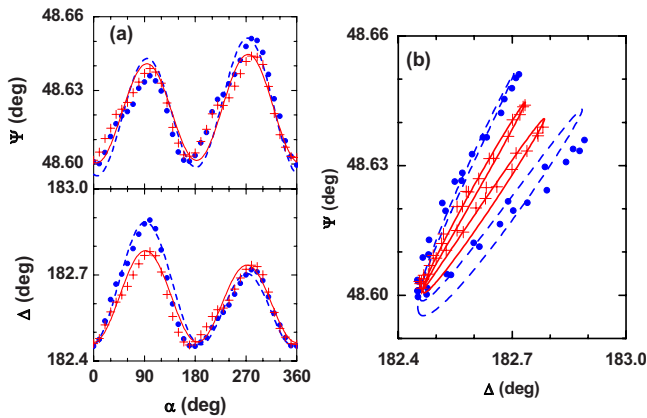
FIG. 5. (Color online) (a) Ψ and Δ vs α for SmST_3 in a 21 layer film. (b) shows Ψ vs Δ. Crosses (circles) represent data and solid (dashed) lines represent simulation results at 93.64 °C (92.66 °C).
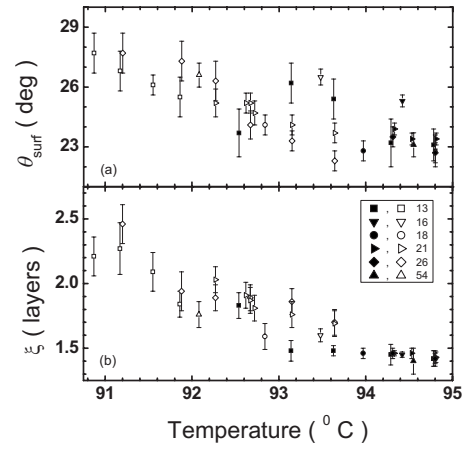
FIG. 6. (a) Surface tilt θ_{surf} and (b) tilt correlation length ξ vs temperature. The points were obtained from simulations. Closed (open) symbols represent data from the SmST_2 (SmST_3) phase. Different symbols correspond to different film thicknesses.

Figs. 4 and 5(b) have two loops. The angle $\varphi_2 - \varphi_1$ is determined by the angle between the two loops of the Ψ vs Δ curve. The correlation length ξ affects the relative length of the two loops of the Ψ vs Δ curve by altering the asymmetry between the two minima of the Ψ and Δ vs α curves.

As temperature decreases, the surface tilt and correlation length increase (Fig. 6). In general, θ_{surf} and ξ should increase as power laws below some critical temperature at which the surface layers begin to tilt. Within the temperature range studied, the increase is approximately linear. This agrees with the fact that the transition temperature for the onset of tilt in surface layers is much higher than the temperatures studied. The correlation length increases from 1.4 layer at $T = 94.8$ °C to about 2.4 layers at $T = 90.8$ °C. The magnitude of the correlation length confirms the earlier observation that there are approximately three layers per surface with measurable tilt angles.

The tilt directions of the interior layers also change with temperature, as shown in Fig. 7. SmST_2 and SmST_3 are both nearly antiferroelectric, meaning that the interior layers' $\vec{c}$ vectors are nearly antiparallel to the $\vec{c}$ vector of the outermost layer in the nearest surface. In SmST_2, the angle $\varphi_2 - \varphi_1$, measured counterclockwise from $\vec{c_1}$ to $\vec{c_2}$ as shown in Fig. 3, is greater than 180°. As temperature decreases within
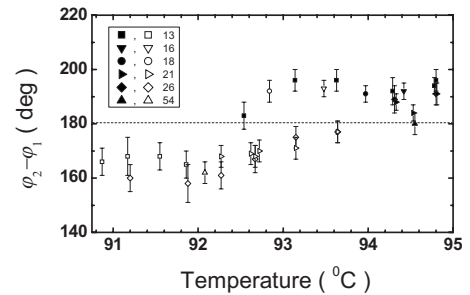
FIG. 7. The nonplanar angle $\varphi_2 - \varphi_1$ vs temperature. The points were obtained from simulations. Closed (open) symbols represent data from the SmST_2 (SmST_3) phase. Different symbols correspond to different film thicknesses.
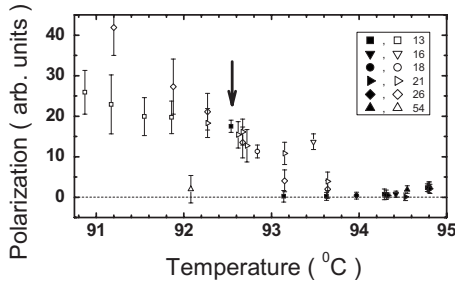
FIG. 8. Net ferroelectric polarization vs temperature. The points were obtained from simulations. The net ferroelectric polarization is proportional to the sum of the $\vec{c}$ vectors for each layer. Closed (open) symbols represent data from the $SmST_2$ ($SmST_3$) phase. Different symbols correspond to different film thicknesses.

the $SmST_2$ window, the structure generally evolves toward a planar arrangement; $\varphi_2 - \varphi_1$ decreases toward 180°. In $SmST_3$, the angle $\varphi_2 - \varphi_1$ is generally less than 180°. Two exceptions to this were observed in 16 and 18 layer films, in which $\varphi_2 - \varphi_1$ remained greater than 180° in $SmST_3$. The direction of $\vec{c_2}$ evolves from one side of the tilt plane of the outermost layers to the other side as temperature decreases. This could also be described as a change in the sign of $\vec{c_1} \times \vec{c_2}$, or a change in the handedness of the structure. The point at which $\vec{c_2}$ is antiparallel to $\vec{c_1}$, corresponding to a planar tilt structure, coincides with the $SmST_2$-$SmST_3$ transition in most of the films studied. As temperature decreases further away from the $SmST_2$-$SmST_3$ transition, the angle $\varphi_2 - \varphi_1$ decreases and the structure evolves away from the planar arrangement.

Any changes in the surface structure with temperature are accompanied by a change in the net polarization of the film. We have obtained the ferroelectric polarizations in Fig. 8 by adding the $\vec{c}$ vectors from our simulation results. The polarization is small in $SmST_2$ and generally decreasing as temperature decreases. One exceptional point from a 13 layer film at 92.54 °C, marked by an arrow in Fig. 8, will be discussed in Sec. IV. In $SmST_3$ the polarization is an order of magnitude larger than in $SmST_2$ and increasing as temperature decreases. The ferroelectric polarization of each layer is approximately proportional to the tilt angle. Because the tilt in each layer is proportional to θ_{surf}, the ferroelectric polarization of each layer is also approximately proportional to θ_{surf}. The polarization of $SmST_2$ is small because the structure is antiferroelectric. The contribution to the net polarization from the outermost layers is slightly larger than the contribution from all of the interior layers, which is in the opposite direction. As the correlation length increases, the polarization of the interior layers increases faster than the polarization of the outermost layers, so the net polarization decreases. Evolution of $\varphi_2 - \varphi_1$ toward 180° also decreases the polarization of $SmST_2$ because the components of the $\vec{c}$ vectors along the direction antiparallel to $\vec{c_1}$ increase. In $SmST_3$, the polarizations of the anticlinic outermost layers cancel, leaving the net polarization due only to the interior layers. This results in a larger net polarization than in $SmST_2$ because the dominant contribution to the net polarization is not counteracted by another contribution in the opposite direction. Increasing ξ produces an increase in the polarization
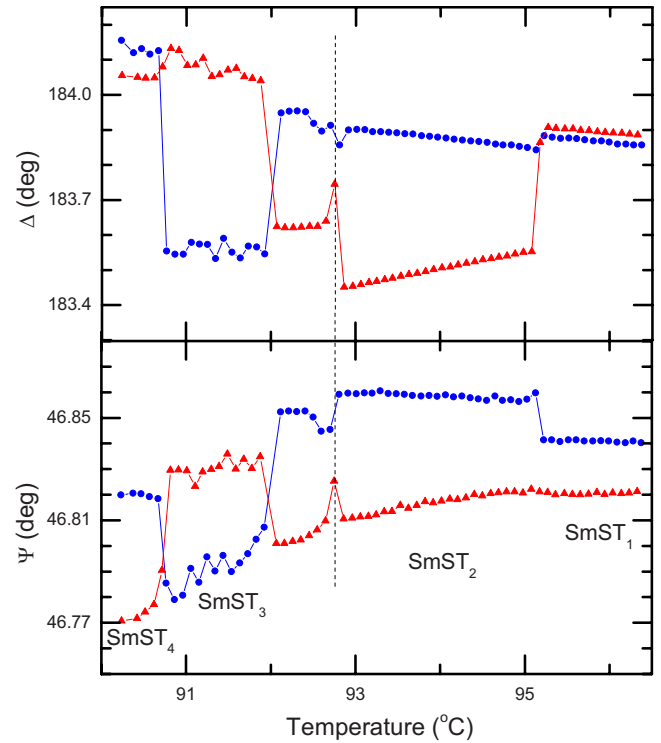
FIG. 9. (Color online) Temperature dependence of Δ and Ψ under two orientations of the electric field for a 13 layer film while cooling at a rate of 20 mK/min. Circles are data obtained at $\alpha = 0°$ and triangles are data obtained at $\alpha = 90°$. The vertical dashed line marks the temperature at which the film structure rotated by 180°, as described in the text.

of the interior layers and in the net polarization. In $SmST_3$, the polarization from the interior layers is due to the components of the $\vec{c}$ vectors perpendicular to the tilt plane of the outermost layers. As $\varphi_2 - \varphi_1$ decreases away from 180°, the structure moves away from a planar arrangement and the polarization increases.

IV. MECHANISMS FOR REORIENTATION OF SURFACE STRUCTURES

In addition to evolution of the surface structures, we have found that the direction of the polarization reverses as temperature changes in $SmST_2$ for 13 layer films. Figure 9 shows NTE data collected while temperature was ramped at a rate of 20 mK/min. The electric field orientation was switched between $\alpha = 0°$ and $\alpha = 90°$ every 2.5 min during the run in order to obtain Ψ and Δ vs temperature for each of these orientations. Between 92.1 °C and 95.1 °C, $\Delta_{90} < \Delta_0$ and $\Psi_{90} < \Psi_0$. This indicates that both Δ and Ψ vs α have minima at $\alpha = 90°$, as seen in Fig. 4. The surface structure is $SmST_2$ through this entire temperature range; however, both Ψ and Δ show a notable feature at 92.8 °C, marked by a vertical dashed line in Fig. 9. The data in Fig. 4 were obtained at temperatures above and below this feature. Note that the data at 94.77 °C in Fig. 4 has $\Delta_{90} - \Delta_{270} < 0$ and $\Psi_{90} - \Psi_{270} > 0$, while the data at 92.54 °C has opposite signs for $\Delta_{90} - \Delta_{270}$ and $\Psi_{90} - \Psi_{270}$. This shows that the Ψ and Δ vs
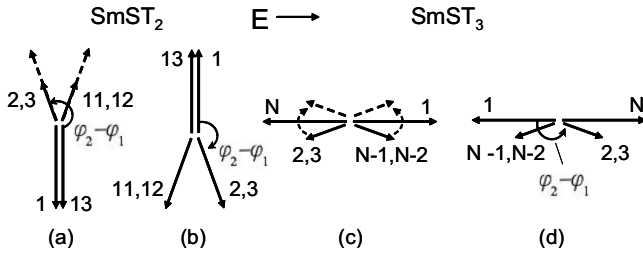
FIG. 10. These diagrams show two mechanisms by which the SmST_2 and SmST_3 structures can rotate by 180°. The SmST$_2$ structures in (a) and (b) have their polarizations aligned with the electric field when the correlation length is small or large, respectively. The dashed arrows in (a) represent an increase in ξ. The SmST$_3$ structures in (c) and (d) have their polarizations aligned with the electric field when $\varphi_2 - \varphi_1 > 180°$ and $\varphi_2 - \varphi_1 < 180°$, respectively. The dashed arrows in (c) represent evolution of φ_2.

FIG. 11. The critical correlation length at which reorientation occurs for a 13-layer film. The line was obtained by setting Eq. (2) equal to zero and solving numerically. See the text for discussion of the dashed arrow.

α curves have shifted by 180°. Meanwhile, the Ψ vs Δ curve in Fig. 4(b) has the same shape, indicating the same structure. The feature marked in Fig. 9 is a rotation of the film structure by 180° about the film normal.

We noted in Sec. III that the polarization in SmST$_2$ decreases as temperature decreases. This occurs because the polarization is approximately proportional to the sum of the $\vec{c}$ vectors. For SmST$_2$,

$$P \propto 2\vec{c}_1 + \sum_{i=2}^{N-1} \vec{c}_i. \tag{2}$$

The factor of 2 in the first term appears because $\vec{c}_1 = \vec{c}_N$ in SmST$_2$. The second term is in the opposite direction from the first term. As temperature decreases, the first term grows approximately linearly as θ_{surf} increases. Meanwhile, the second term increases both due to the increase in θ_{surf} and due to the increase in the tilt correlation length. The second term therefore grows faster than the first term, causing the polarization to decrease. If the correlation length is large enough, the polarization will go to zero then reverse direction. The entire tilt structure must then rotate around the film normal by 180° in order to align the polarization with the applied electric field, such as at the feature marked by the dashed line in Fig. 9. This process is illustrated in Figs. 10(a) and 10(b). For any film thickness and angle $\varphi_2 - \varphi_1$, the condition for reorientation is $P = 0$. The tilt structure when reorientation occurs can be found by setting Eq. (2) equal to zero and solving numerically for the correlation length. Figure 11 shows such a solution for a 13-layer film. For films thicker than a few times ξ, or about 10 layers, any thickness dependence to the solutions of $P = 0$ is negligible, because the tilt does not penetrate all the way to the center of the film. The correlation length at which reorientation occurs increases slightly with $\varphi_2 - \varphi_1$.

From Fig. 7, we can see that for a 13-layer film in SmST$_2$, $\varphi_2 - \varphi_1 \approx 196°$. This angle does not vary rapidly with changes in temperature. The data from simulations for a 13-layer film in Figs. 6 and 7 show that the structure evolves along the dashed arrow in Fig. 11. The molecules in the film reorient by 180° when the dashed arrow crosses the $P = 0$ line at ξ
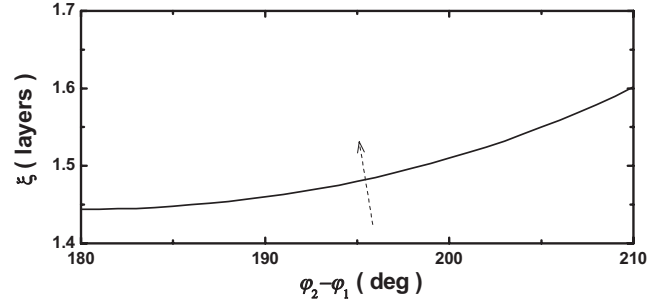
$= 1.485 \pm .005$ layers. By comparison with Fig. 6(b), reorientation is expected to occur at about 93.0 °C. This is in good agreement with the temperature at which reorientation was noted in Fig. 9. Since the value of ξ at which reorientation occurs does not depend on thickness for films thicker than about 10 layers, reorientation is expected at about the same temperature in SmST$_2$ regardless of thickness. We only observed reorientation in a 13-layer film. Other films did not show this feature because in all thicknesses other than 13 layers, the SmST$_2$-SmST$_3$ transition temperature was higher than 93.0 °C.

At temperatures below the point at which reorientation occurs, the behavior of the net polarization with temperature in SmST$_2$ changes. At high temperatures, the first term in Eq. (2) has larger magnitude than the second term. The net polarization decreases as the second term grows. Below the reorientation temperature, the magnitude of the second terms becomes larger. As temperature decreases, the second term grows faster than the first term, so the net polarization increases below the reorientation temperature. This is illustrated by the point marked with an arrow in Fig. 8. This point is for a 13-layer film below the reorientation temperature, for which experimental data is shown in Fig. 4. The net polarization for this point is larger than for the other points in Fig. 8 for SmST$_2$ because the polarization has begun to grow below the reorientation temperature.

The structure for SmST$_3$ may also undergo a 180° reorientation by a different mechanism, although we have not observed a reorientation of SmST$_3$ in our experiments. The nonplanar angle $\varphi_2 - \varphi_1$ evolves with temperature, passing through 180°. In the films that we studied, the temperature at which $\varphi_2 - \varphi_1 = 180°$ coincides with the SmST$_2$-SmST$_3$ transition temperature; however, this needs not be the case. If $\varphi_2 - \varphi_1$ evolves through 180° in SmST$_3$, a 180° reorientation of the film structure should occur. The mechanism is illustrated in Figs. 10(c) and 10(d). Since SmST$_3$ is anticlinic, the polarizations of the outermost layers cancel and the net polarization is due only to the interior layers. Moreover, only the components of the $\vec{c}$ vectors of the interior layers that are perpendicular to the tilt plane of the outermost layers contribute to the net polarization. If $\varphi_2 - \varphi_1$ goes to 180°, the net polarization goes to zero. Thus, if $\varphi_2 - \varphi_1$ passes through 180° in SmST$_3$, the film structure should rotate by 180° about the film normal to align the polarization with the applied electric field.
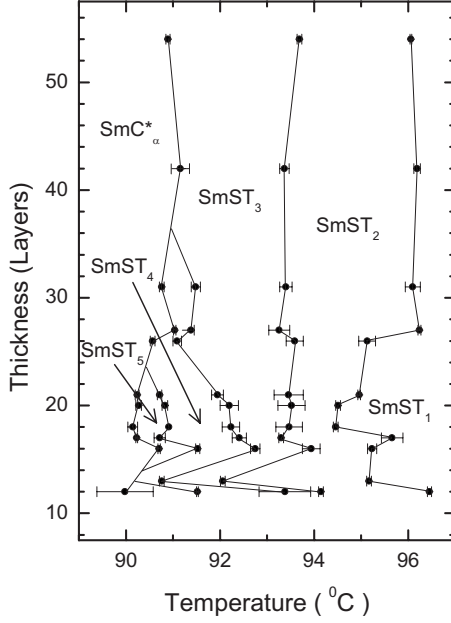
FIG. 12. Phase diagram for the five surface phases. The error bars represent the range of hysteresis in the transition temperatures during heating and cooling temperature ramps.

V. SURFACE PHASE DIAGRAM

A phase diagram displaying the dependence of the five surface structures on temperature and film thickness is shown in Fig. 12. No surface structures in the bulk SmA temperature region were observed other than the five structures previously reported for a 16-layer film. The SmST_1 structure persists up to the bulk SmA-Isotropic transition. As film thickness increases, the SmST_1-SmST_2, SmST_2-SmST_3, and bulk SmA-SmC_α^* transition temperatures remain approximately constant. SmST_1, SmST_2, and SmST_3 are observed even in films as thick as about 100 layers. However, SmST_4 and SmST_5 disappear from the phase diagram as thickness increases. SmST_5 does not occur in films thicker than about 23 layers and SmST_4 disappears in films thicker than about 35 layers.

The surface structures are controlled by three interactions: short-range interactions between nearest neighbor and next nearest neighbor layers in one surface [18,19], a dipole-dipole interaction between the polarizations of the top and bottom surfaces of the film, and long-range elastic interactions [20]. An interaction of the net polarization with the applied electric field is also present; however, we have observed that the transition temperatures are equal to within our resolution for applied electric fields of 0.14, 7, or 14 V/cm. We therefore expect that the interaction with the applied electric field used in our studies is unimportant for all of the surface transitions. The short-range interactions determine whether the surfaces are ferroelectric or antiferroelectric. These interactions do not depend on film thickness as long as the film is thick enough to contain a SmA bulk.

The dipole-dipole interaction between the polarizations of the two surfaces affects the synclinic or anticlinic arrangement of the outermost surfaces. This interaction is favorable

if the polarizations of the top and bottom surfaces are antiparallel. From the structures shown in Fig. 3, it is readily apparent that the surface polarizations are nearly parallel and unfavorable in SmST_1 and SmST_4 and nearly antiparallel and favorable in SmST_5. Adding the $\vec{c}$ vectors for SmST_2 and SmST_3 using the fit parameters shows that dipole-dipole interactions are only slightly favorable for SmST_2 and approximately zero for SmST_3. The dipole-dipole interaction strength decreases as film thickness increases.

Elastic interactions arise from spatial gradients of the director $\hat{n}$. In a planar structure, elastic deformations are pure bend deformations due to variation in the tilt angle with depth from the surface. In these nonplanar structures, the elastic energy is still primarily due to bend deformations, with minor contributions from splay and twist deformations. The elastic free energy density is largest where the gradient of the tilt angle is largest, near the surfaces of the film. Therefore, the elastic free energy is nearly independent of film thickness, as long as the film is thick enough to contain a SmA bulk. To compare the elastic energy of each surface structure, we consider the Frank free energy in the one constant approximation.

$$F = \frac{1}{2}K[(\nabla \cdot \hat{n})^2 + (\hat{n} \cdot \nabla \times \hat{n})^2 + (\hat{n} \times \nabla \times \hat{n})^2]$$

$$= \frac{1}{2}K[(\nabla \cdot \hat{n})^2 + (\nabla \times \hat{n})^2]. \tag{3}$$

Discretizing this equation allows for calculation of the elastic free energy for each surface structure. The elastic free energy increases by a factor of approximately 2 when the surface structure changes from SmST_1 to SmST_2 and decreases by a factor of approximately 2 when the surface structures changes from SmST_3 to SmST_4. At the other surface structure transitions, the elastic free energy does not change appreciably.

At the SmST_1-SmST_2 transition, the structure changes from synclinic and ferroelectric (SmST_1) to synclinic and antiferroelectric (SmST_2). This transition is governed by the short-range interactions. Though not fully understood, the short-range interactions are expected to depend on the tilt angle, which in turn depends on temperature. Film thickness, on the other hand, is not expected to have a significant effect. The transition should occur at the same temperature, regardless of the film thickness. The phase diagram is in good agreement with this.

A change from synclinic to anticlinic outermost layers characterizes the SmST_2-SmST_3 transition. The angles between adjacent layers within each surface are unchanged, so the short-range interactions are not expected to play a role in this transition. The elastic energy also remains approximately constant. The SmST_2-SmST_3 transition is driven by the dipole-dipole interaction between the opposite surfaces of the film. If the correlation length is small, the antiferroelectric surfaces in SmST_2 and SmST_3 have ferroelectric polarizations that are dominated by the outermost layer. As the correlation length grows, the polarization of each surface evolves, changing to the opposite direction when the correlation length is large. In SmST_2, the dominant contribution to

the ferroelectric polarization is due to the components of the $\vec{c}$ vectors of the interior layers that are perpendicular to the tilt plane of the outermost layers. The opposite surfaces then have polarizations that are nearly antiparallel, as favored by the dipole-dipole interactions. In SmST_3, the correlation length is larger so the dominant contribution to the ferroelectric polarization of each surface is due to the component of the $\vec{c}$ vectors of the interior layers parallel to the tilt plane of the outermost layers. The surfaces reorient so that the $\vec{c}$ vectors of the interior layers are nearly antiparallel in order to minimize the dipole-dipole interaction energy. The correlation length is the determining factor for this transition, so the transition temperature is not expected to depend on film thickness.

As the surface structure changes from SmST_3 to SmST_4, the polarizations of the surfaces revert to the synclinic arrangement that is disfavored by the dipole-dipole interactions. The elastic energy is lower in SmST_4 than in SmST_3. The SmST_3-SmST_4 transition occurs at the temperature for which the difference in the elastic energy is equal to the difference in the dipole-dipole energy. Since the elastic energy is nearly independent of film thickness, but the dipole-dipole interaction energy is proportional to $1/N^3$, the SmST_3-SmST_4 transition temperature is expected to increase in thicker films. However, the phase diagram shows that SmST_3 persists to lower temperature in thicker films. This discrepancy is not well understood. In addition, the outermost layers and their adjacent layers revert back to a ferroelectric arrangement at the SmST_3 to SmST_4 transition. This means that the short-range interactions play some role in the SmST_3-SmST_4 transition. It is not understood why the short-range interactions produce a reentrant ferroelectric-antiferroelectric-ferroelectric transition.

The SmST_4-SmST_5 transition is similar to the SmST_2-SmST_3 transition, in that the structures changes from synclinic to anticlinic. Just as for the SmST_2-SmST_3 transition, the short-range interactions and the elastic interactions have no effect. Each surface has a polarization due to the outermost layers and the interior layers. The SmST_4-SmST_5 transition occurs because growth of the correlation length causes the polarization of the interior layers to grow. When the correlation length is larger, in SmST_5, the dipole-dipole interactions are minimized so that the tilts of the interior layers are nearly antiparallel.

VI. CONCLUSIONS

The unusual sequence of surface transitions in the bulk SmA temperature window of 12OF1M7 has proven to be surprisingly robust with respect to changes in temperature and film thickness. For different film thicknesses, the same five surface structures occur in the same sequence. The primary effect of changing the film thickness is to remove some of the surface phases from the sequence. This sequence of surface transitions is fairly complicated and not completely understood. Even in this system, some features of the surface phase diagram can be explained by considering elastic deformations, short-range interactions, and dipole-dipole interactions.

We have performed detailed simulations to obtain the magnitude and direction of the surface tilts in the SmST_2 and SmST_3 phases. The surface tilt and the correlation length increase as temperature decreases, consistent with expectations. In addition, the direction of the tilt of the interior layers evolves with temperature, passing through a planar state at a temperature that coincides with the SmST_2-SmST_3 transition temperature in most films. Changes in the magnitude and direction of the tilt and in the correlation length also affect the polarization. We have shown that typically $dP/dT < 0$ in SmST_2 and $dP/dT > 0$ in SmST_3. In some situations, the net polarization can pass through zero and change direction due to changes in either the correlation length or the tilt direction of the interior layers. The same techniques used here could be applied to other compounds. In particular, studies of thin films or compounds with simpler surface structures may yield important information about the interactions between molecules in smectic phases.

[1] P. G. DeGennes and J. Prost, *The Physics of Liquid Crystals* (Clarendon Press, Oxford, 1993).

[2] R. Hołyst, Phys. Rev. A **44**, 3692 (1991).

[3] Ch. Bahr and D. Fliegner, Phys. Rev. Lett. **70**, 1842 (1993).

[4] P. M. Johnson, D. A. Olson, S. Pankratz, Ch. Bahr, J. W. Goodby, and C. C. Huang, Phys. Rev. E **62**, 8106 (2000).

[5] B. Rovšek, M. Čepič, and B. Žekš, Phys. Rev. E **66**, 051701 (2002).

[6] S. T. Wang, X. F. Han, Z. Q. Liu, A. Cady, M. D. Radcliffe, and C. C. Huang, Phys. Rev. E **68**, 060702(R) (2003).

[7] X. F. Han, D. A. Olson, A. Cady, D. R. Link, N. A. Clark, and C. C. Huang, Phys. Rev. E **66**, 040701(R) (2002).

[8] B. K. McCoy, Z. Q. Liu, S. T. Wang, V. P. Panov, J. K. Vij, J. W. Goodby, and C. C. Huang, Phys. Rev. E **73**, 041704 (2006).

[9] B. K. McCoy, Z. Q. Liu, S. T. Wang, Lidong Pan, Shun Wang, J. W. Goodby, and C. C. Huang, Phys. Rev. E **79**, 061702 (2009).

[10] C. Y. Chao, C. R. Lo, P. J. Wu, Y. H. Liu, D. R. Link, J. E. Maclennan, N. A. Clark, M. Veum, C. C. Huang, and J. T. Ho, Phys. Rev. Lett. **86**, 4048 (2001).

[11] X. F. Han, S. T. Wang, A. Cady, M. D. Radcliffe, and C. C. Huang, Phys. Rev. Lett. **91**, 045501 (2003).

[12] D. R. Link, G. Natale, N. A. Clark, J. E. Maclennan, M. Walsh, S. S. Keast, and M. E. Neubert, Phys. Rev. Lett. **82**, 2508 (1999).

[13] D. A. Olson, X. F. Han, P. M. Johnson, A. Cady, and C. C. Huang, Liq. Cryst. **29**, 1521 (2002).

[14] D. W. Berreman, J. Opt. Soc. Am. **62**, 502 (1972); H. Wohler, G. Haas, M. Fritsch, and D. A. Mlynski, J. Opt. Soc. Am. A **5**, 1554 (1988).

[15] D. A. Olson, S. Pankratz, P. M. Johnson, A. Cady, H. T. Nguyen, and C. C. Huang, Phys. Rev. E **63**, 061711 (2001).

[16] V. P. Panov, B. K. McCoy, Z. Q. Liu, J. K. Vij, J. W. Goodby, and C. C. Huang, Phys. Rev. E **74**, 011701 (2006).

[17] Ch. Bahr, C. J. Booth, D. Fliegner, and J. W. Goodby, Phys. Rev. E **52**, R4612 (1995).

[18] D. A. Olson, X. F. Han, A. Cady, and C. C. Huang, Phys. Rev. E **66**, 021702 (2002).

[19] P. V. Dolganov, V. M. Zhilin, V. K. Dolganov, and E. I. Kats, Phys. Rev. E **67**, 041716 (2003).

[20] D. Schlauf, Ch. Bahr, and H. T. Nguyen, Phys. Rev. E **60**, 6816 (1999).